29B X-734-67-321 END

29A NASA-TM X-55850 29B

3

PARAMETRIC ANALYSIS OF ELECTROSTATIC DISPERSION OF A LIQUID 6

JULY 1967

NASA — GODDARD SPACE FLIGHT CENTER —
GREENBELT, MD.

X-734-67-321

PARAMETRIC ANALYSIS OF ELECTROSTATIC DISPERSION OF A LIQUID

Allan Sherman
Auxiliary Propulsion Branch

July 1967

GODDARD SPACE FLIGHT CENTER
Greenbelt, Maryland

PARAMETRIC ANALYSIS OF ELECTROSTATIC DISPERSION OF A LIQUID

Allan Sherman
Auxiliary Propulsion Branch

ABSTRACT

This document presents a theoretical model for the electrostatic dispersion of a fluid. The analysis results in equations for charge-to-mass ratio, velocity, and droplet radius as a function of flow-voltage parameters. Data from colloid rocket tests agree favorably with theory. The results are useful for colloid-rocket data correlation.

CONTENTS

PRECEDING PAGE BLANK NOT FILMED.

ILLUSTRATIONS

NOTATIONS

A	flow area of capillary (m^2)
C	wave velocity
D	diameter of capillary (m)
$f(\epsilon, \rho)$	function of dielectric constant and density of fluid
G	defined by equation (9)
L	length of capillary (m)
N	number of drops/second leaving fluid surface
P	permittivity of fluid (f/m)
Q/M	charge-to-mass ratio of droplet (coul/kg)
R	radius of droplet (m)
R_i	radius of perturbation
V	voltage (volts)
v	velocity (m/sec)
V_0	volume
ΔP_σ	pressure rise or drop across meniscus
ϵ	fluid dielectric constant
ρ	fluid density (kg/m^3)
σ	surface tension (dynes/cm)
ω	flow (kg/sec)

PARAMETRIC ANALYSIS OF ELECTROSTATIC DISPERSION OF A LIQUID

INTRODUCTION

The electrostatic dispersion of a fluid is a complicated physical process for which no simplified theoretical model has been presented. This analysis is an attempt to present a theoretical model which can be used to predict droplet radius, charge-to-mass ratio, and velocity, and to identify significant flow-dispersion parameters. The results are particularly applicable to analysis and evaluation of colloid rocket performance.

The approach employed in this analysis is to examine the meniscus (liquid surface-environment interface) and to devise a model for droplet growth and expulsion, with appropriate equations. Then, experimental data are compared with the theoretical predictions to validate the model.

THEORY

General Description of Flow

Figure 1 illustrates the overall flow process in the colloid-rocket capillary where P_1 is the liquid feed pressure, P_2 is the pressure on the liquid side of the meniscus, P_3 is the environmental pressure, and V is the applied voltage.

The pressure drop in the capillary is related to the flow by the Hagen-Poiseuille relationship:

$$P_1 - P_2 = f L/D \dot{\omega}^2/2\rho A^2 \qquad (1)$$

where $f = 64/Re$ for laminar flow. The pressure drop or rise across the meniscus is fixed by the La Place-Young equation:

$$\Delta P_\sigma = \frac{2\sigma}{R_{cv}} \qquad (2)$$

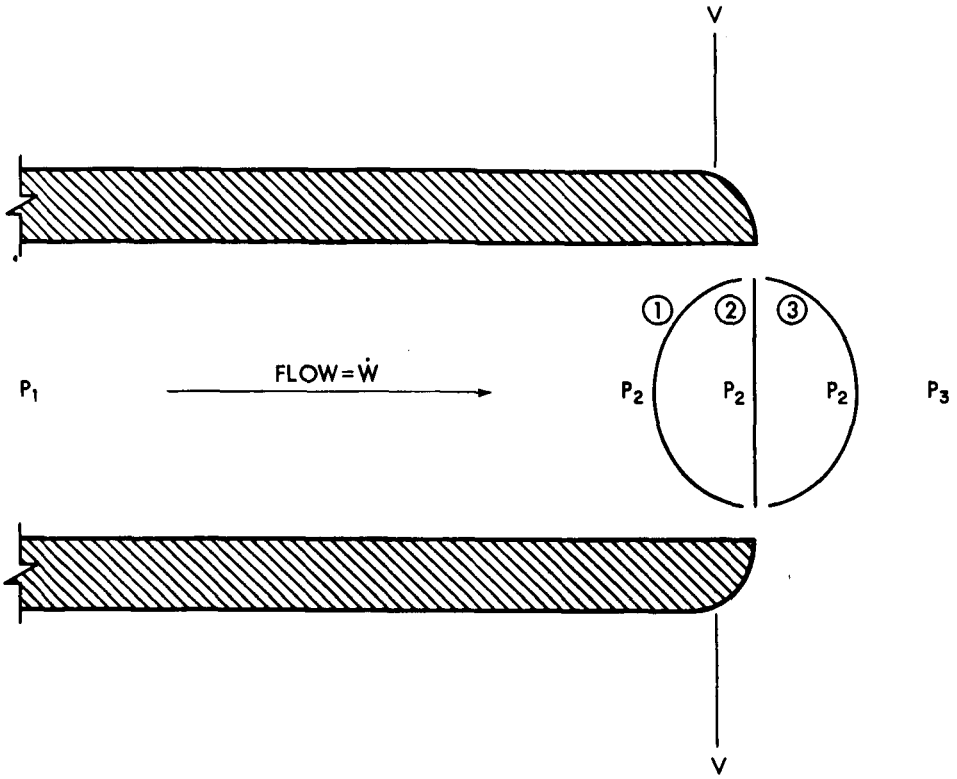

① - MENISCUS FOR $P_3 > P_2$
② - MENISCUS FOR $P_3 = P_2$
③ - MENISCUS FOR $P_3 < P_2$

$\dot{W}_1 > \dot{W}_2 > \dot{W}_3$

Figure 1. Overall Meniscus Shapes in Flow Capillary

where R_{cv} is the radius of curvature at the interface. If the meniscus is convex with respect to the liquid (case 3 in Figure 1), the liquid pressure P_2 is greater than the environmental pressure; if the meniscus is concave with respect to the liquid, the liquid pressure is less than the environmental pressure. By using equations (1) and (2), the operation of the needle can be visualized. Suppose P_1 is raised to a point where the pressure forces balance the surface tension forces, just before the onset of flow: The meniscus would then assume position 3 in Figure 1 with $P_1 = P_2$. If a small voltage is applied, resulting in a flow, P_2 falls below P_1 (equation (1)) and closer to P_3. As the voltage and flow are further increased, P_2 will decrease below P_3, resulting in position 1 in Figure 1 (equation (2)). If the voltage is increased even more, the meniscus will reach a position from which it can recede no more (because of contact-angle and surface-energy effects). After this point, the flow will not increase

with voltage, and hence is fixed with P_1. A colloid-rocket propulsion system would ordinarily operate in this regime.

Analysis

Figure 2 shows a perturbation, or microscopic fluctuation, on the meniscus of the fluid in the capillary, where R_i is the initial radius of the assumed hemispherical fluctuation.

The condition for growth of the perturbation is

$$Pe > \Delta P_\sigma \tag{3}$$

where ΔP_σ is defined by equation (2) for R_i, and P_e is the electrostatic pressure in the perturbation.

Assuming the hemispherical perturbation, the electrostatic pressure can be expressed by

$$Pe = \frac{V^2}{7.4 \times 10^5 \pi R_i^2} f(\epsilon, \rho)^{[1]} \tag{4}$$

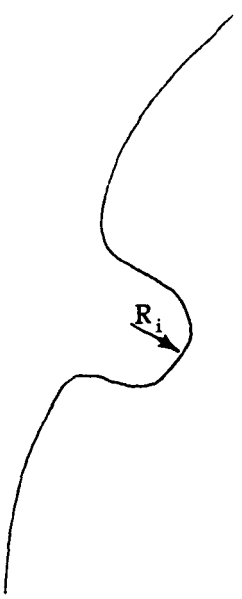

Figure 2. Perturbation of Meniscus

with the following assumptions:

- The specific electrical conductivity of the fluid is less than 10^{-5} mho /cm.
- The dielectric constant of the liquid perturbation in the transition surface layer changes continuously from a value of E in the interior to 1 in air or vacuum, and the transition thickness is about equal to the liquid dipole length.

The factor $f(\epsilon, \rho)$ can be determined for many fluids by the methods of Henriquez [2] and Onsager [3].

Substituting equations (4) and (2) into (3) yields

$$\frac{V^2}{7.4 \times 10^5 \pi R_i^2} f(\epsilon, \rho) > \frac{2\sigma}{R_i} \tag{5}$$

for perturbation growth. Equation (5) may be rewritten as

$$R_i < \frac{V^2}{14.8 \times 10^5 \pi\sigma} f(\epsilon, \rho) \ . \tag{6}$$

Equation (6) states a condition for growth of a perturbation; i.e., all perturbations of R_i less than $V^2/(14.8 \times 10^5 \pi\sigma\, f(\epsilon, \rho))$ will grow, while all perturbations greater than this factor will not. Figure 3 illustrates a distribution curve (type unknown) for the perturbations; at voltage V_1, all perturbations less than $R_{i\,max_1}$ will grow, and at V_2 all perturbations less than $R_{i\,max_2}$ will grow. For each case, the total number of perturbations per second that will grow is expressed by

$$N = \int_0^{R_{i\,max}} N_p \, dR_i \tag{7}$$

and hence N = area under the distribution curve to the specified limits.

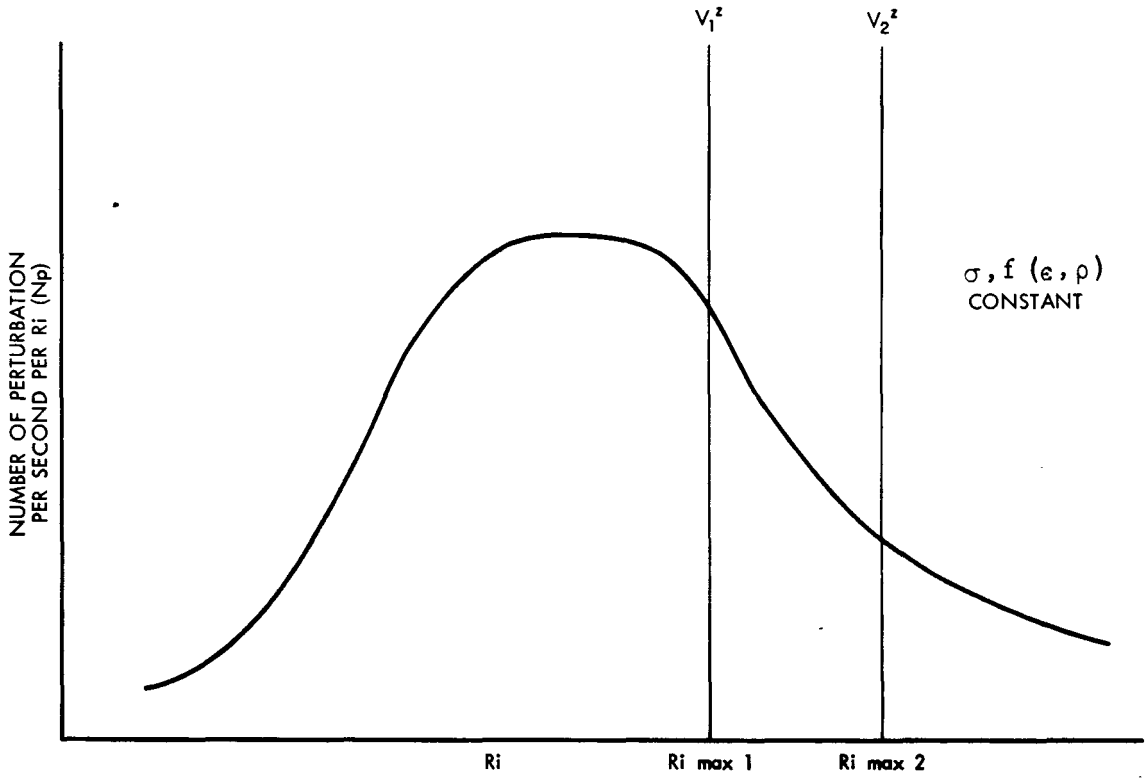

Figure 3. Perturbation Distribution Curve

From equations (6) and (7), and Figure 3:

$$N \propto G \frac{V^2}{\sigma} f(\epsilon, \rho) \tag{8}$$

where G is a function of the particular perturbation distribution for the meniscus of concern.

Because the distribution curve is unknown, as a first-order approximation it will be assumed that G is constant for a given fluid. This in effect assumes a flat distribution within the limits of interest. Hence,

$$N = G \frac{V^2}{\sigma} f(\epsilon, \rho) \quad . \tag{9}$$

Assuming the droplets leaving the liquid surface are of equal size (if they are not, then we are considering an average drop),

$$\dot{\omega} = NM$$

$$= N(4/3\,\pi R^3 \rho) \tag{10}$$

for a spherical drop.

Combining equations (10) and (9) and solving for R yields

$$R = 3\sqrt{\frac{3}{4}\frac{\dot{\omega}}{K V^2 \pi \rho}} \tag{11}$$

where

$$k = G/\sigma\, f(\epsilon, \rho)$$

The exact mechanism for the expulsion of a droplet from the surface of the fluid is unknown. However, Figure 4 is a simplified model of the process which consists of a perturbation growing from R_i to R, with breakoff at R. At breakoff, half the droplet is formed and an equal mass of fluid is extracted from the fluid bulk.

With this model, the charge on the droplet at breakoff can be calculated by

$$Q = (2\pi R^2)\, P(V/R)$$

$$= 2\pi R VP \tag{12}$$

where P is the permittivity of the fluid.

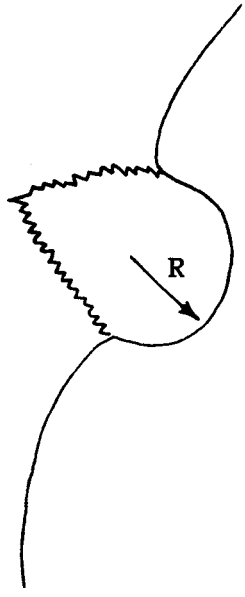

Figure 4. Model for Drop Breakoff

The charge-to-mass ratio of a droplet is

$$\frac{Q}{M} = \frac{2RVP}{4/3\,\pi R^3 \rho} = \frac{3}{2}\frac{VP}{\pi R^2 \rho} \cdot \tag{13}$$

Substitution of equation (11) into (13) yields

$$\frac{Q}{M} = K_1 \frac{U^{7/3}}{\dot{\omega}^{2/3}} \tag{14}$$

where

$$K_1 = 1.82 \frac{P K^{2/3}}{\rho^{1/3} \pi^{1/3}} \cdot$$

The energy equation for the liquid droplet, assuming small viscous dissipation and droplet surface energy, is

$$QV = \frac{1}{2} M v^2 \quad . \tag{15}$$

Hence,

$$v = \sqrt{2 \frac{Q}{M} V} \quad . \tag{16}$$

Combining equations (16) and (14) yield

$$v = \sqrt{2K_1} \frac{V^{5/3}}{\dot{\omega}^{1/3}} \quad . \tag{17}$$

Equations (9) through (17) show that for a known G the significant flow parameters (charge-to-mass ratio, droplet size, velocity, etc.) can be calculated. Thus, within the bounds of the theoretical model, G is a parameter of prime significance.

DATA CORRELATION

Little data are available to fulfill the initial assumption of a conductivity less than 10^{-5} mho/cm. The best data found were from twenty-three tests run with sodium hydroxide-doped glycerol (resistivity = 7215 ohm-cm) from reference (6).

The parameters Q/M, V, and $\dot{\omega}$ were measured during these tests, and G could be calculated from equation (14) for each point. Figure 5 shows the results of these calculations, which indicate that G is not a function of flow (P_1) and shows no discernable variation with voltage. Hence, the assumption of constant G is validated, although there is some scatter in these data. From these data, G is taken as a constant equal to 1.2.

Using this value for G, the charge-to-mass ratio and velocity of the particles were calculated from equations (14) and (17). Figures 6 and 7 show a comparison between these results and the data.

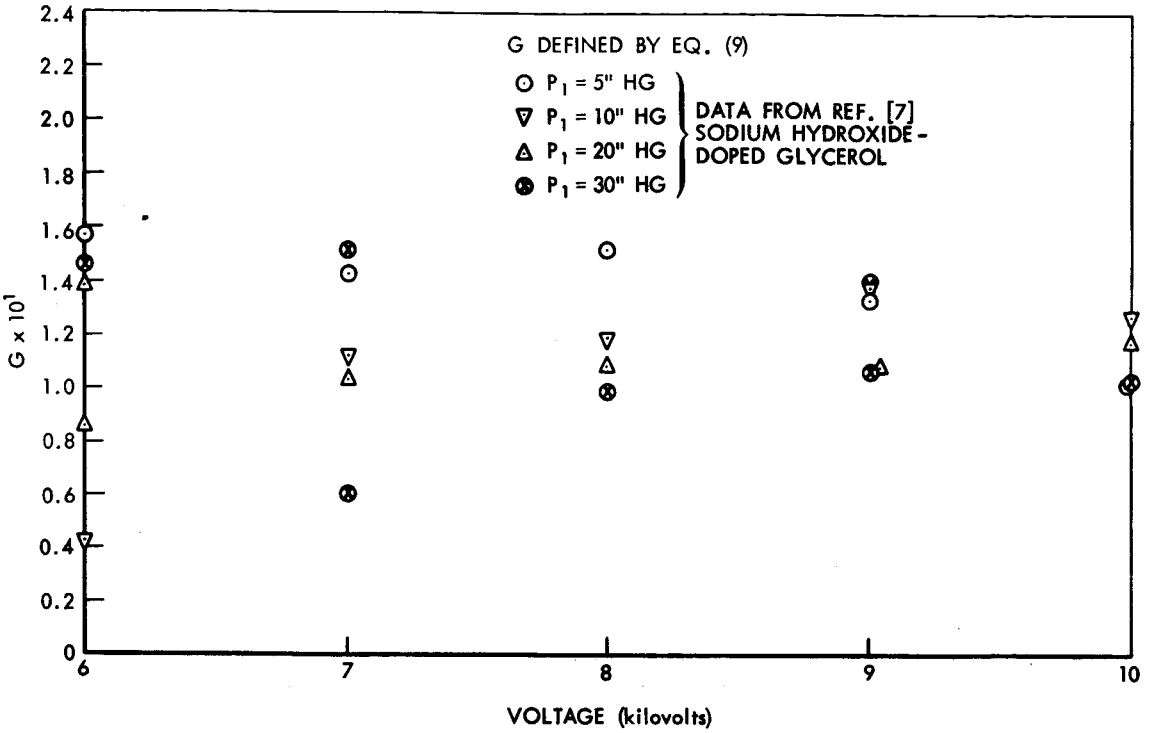

Figure 5. Variation of Parameter G with Voltage

Figure 6 validates equation (14): i.e., Q/M varies linearly with $V^{7/3}/\dot{\omega}^{2/3}$. The assumed model, with constant G, appears to be correct at least within the range of these tests (6 to 10 kv, 0.664×10^{-8} to 4.4×10^{-8} kg/sec).

Figure 7 shows a good correlation with the energy equation. The decrement in the velocity of these data, as compared to theory, arises from slight errors in the reduction of the experimental data. In fact, because the measured charge-to-mass ratio is deduced from the energy equation by measuring the velocity, the agreement between theory and data in Figure 7 should be as good as in Figure 6.

Reference 6 also contains data from tests run with a sodium ethylate-doped glycerol solution. The resistivity of this solution, 3470 ohm-cm, is further away from the initial assumption of a greater than 10^5 ohm-cm resistivity. Nevertheless, Figure 8 shows that equation (14) is valid for this case also.

If, now, the slope of the data in Figure 8 (K_1) is put into equation (17), the velocity of the particles can be calculated. Figure 9 shows the results, in which the difference between theory and data again arises from data-reduction errors.

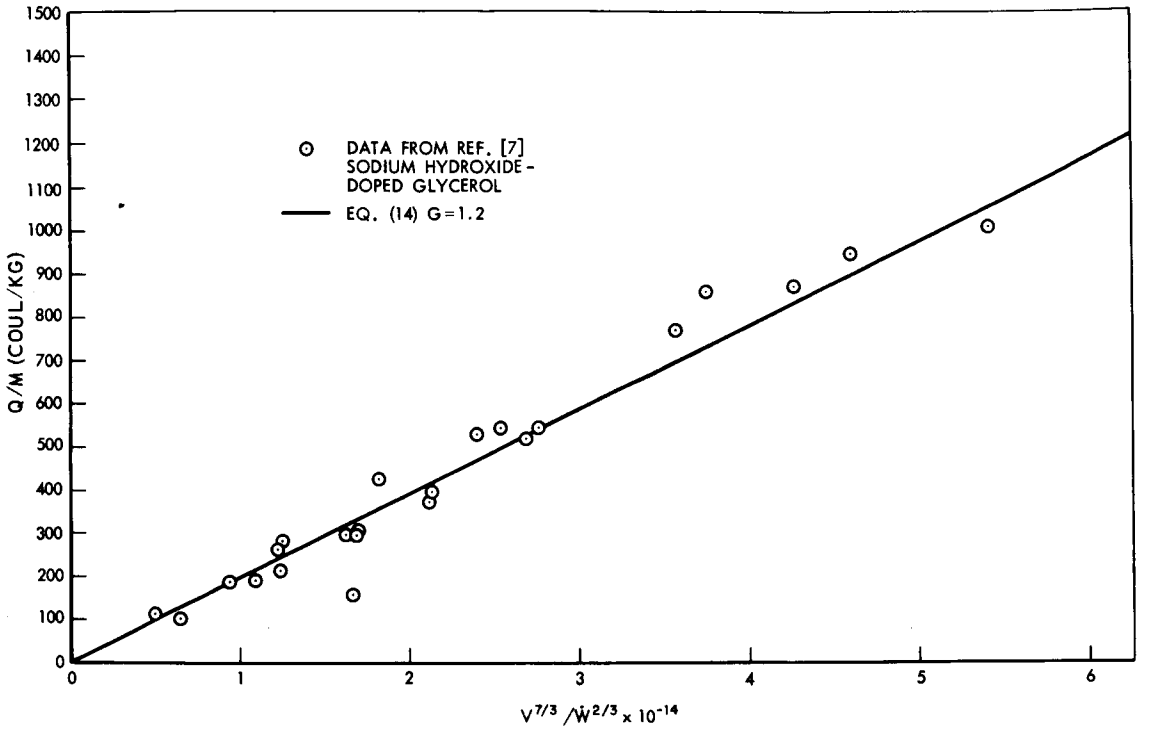

Figure 6. Charge-to-Mass Ratio vs Flow-Voltage Parameter–Fluid 1

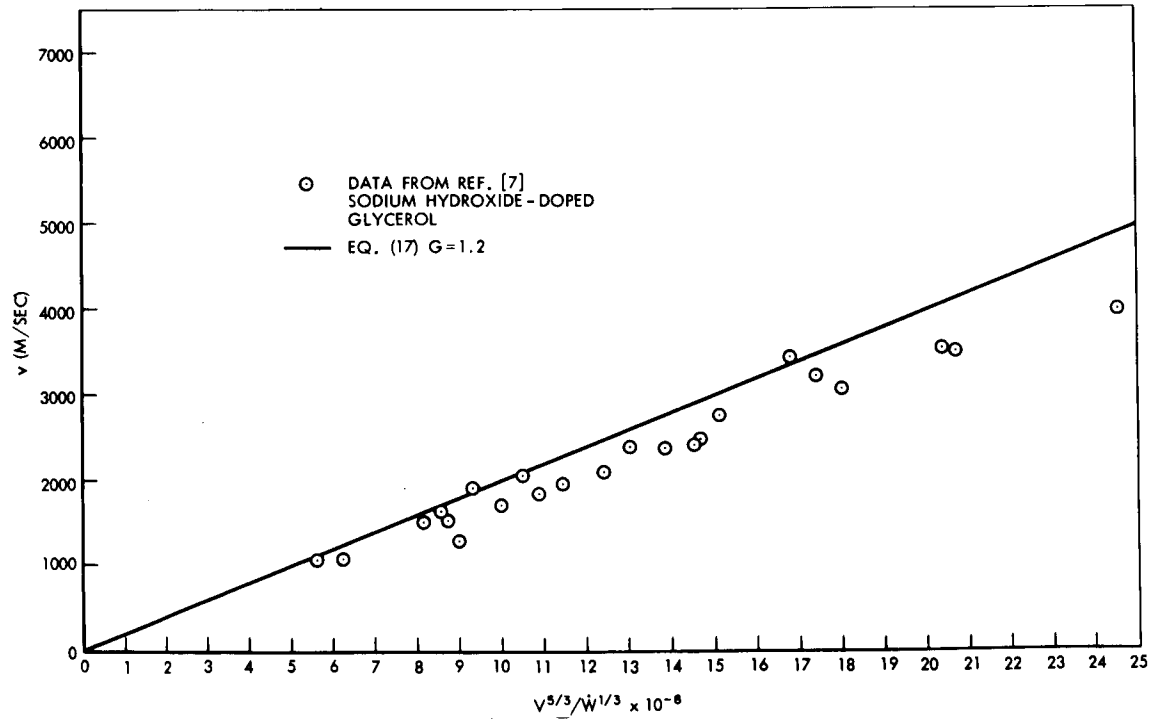

Figure 7. Droplet Velocity vs Flow-Voltage Parameter–Fluid 1

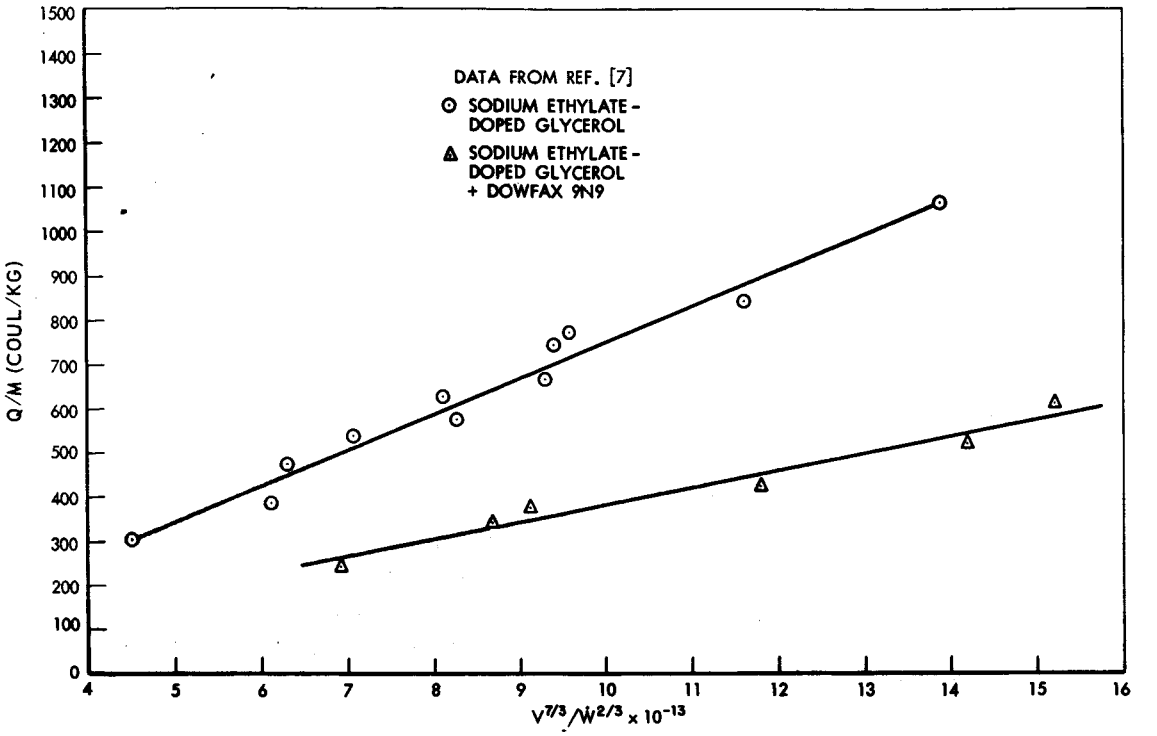

Figure 8. Charge-to-Mass Ratio vs Flow-Voltage Parameter–Fluid 2

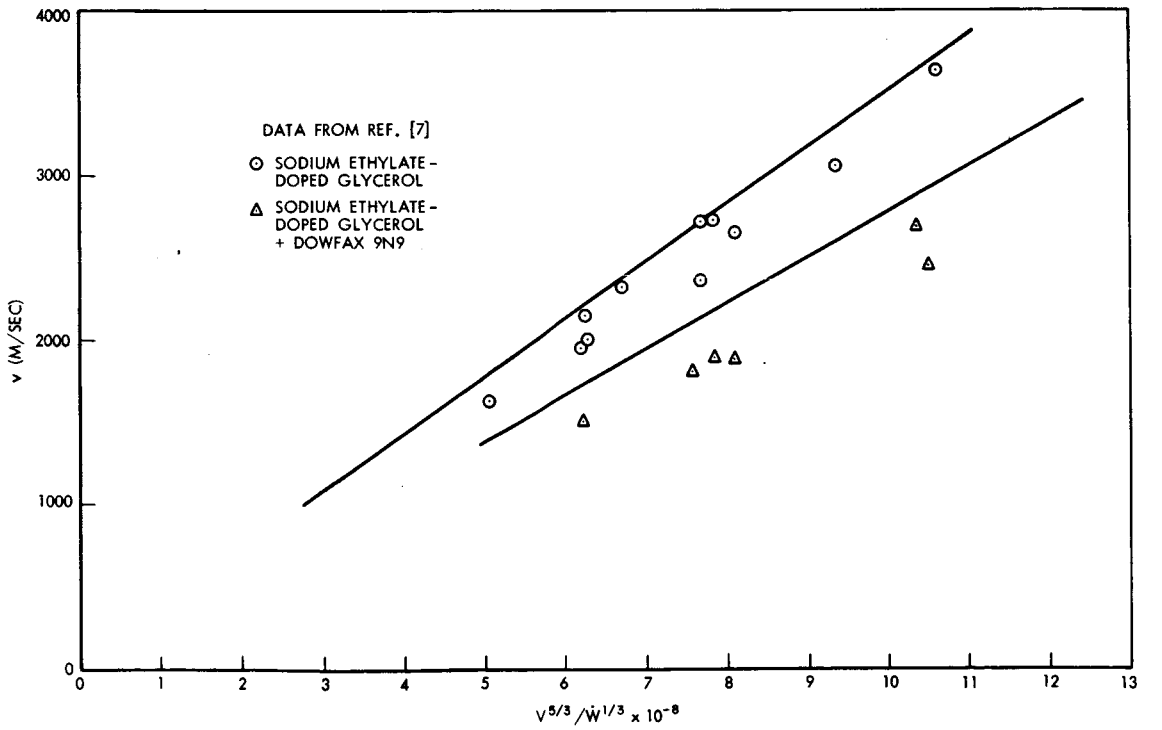

Figure 9. Droplet Velocity vs Flow-Voltage Parameter–Fluid 2

Figure 10 is a plot of equation (11) showing the effect of flow and voltage on droplet radius for the sodium hydroxide-doped glycerol tests from reference 6.

DISCUSSION

Comparison With Other Analysis

In the present analysis, equation (9) is the criterion used to determine droplet radius for a given flow. This method appears more sound than using droplet energy minimization (references 5 and 8) which does not consider the process or energy expended during formation. For example, Pfeifer, in reference 9, computes the charge-to-mass ratio for a droplet by combining an equation for the charge buildup on a growing fluctuation with an energy minimization criteria on the final droplet. The resulting voltage-flow parameter for the calculation of Q/M (to be compared with equation (14)) was $(V/\dot{\omega})^{3/7}$. Figure 11 shows data from reference 7 plotted against this parameter. Comparison of Figures 11 and 6 shows that the model outlined in this report results in a significant improvement in this correlation

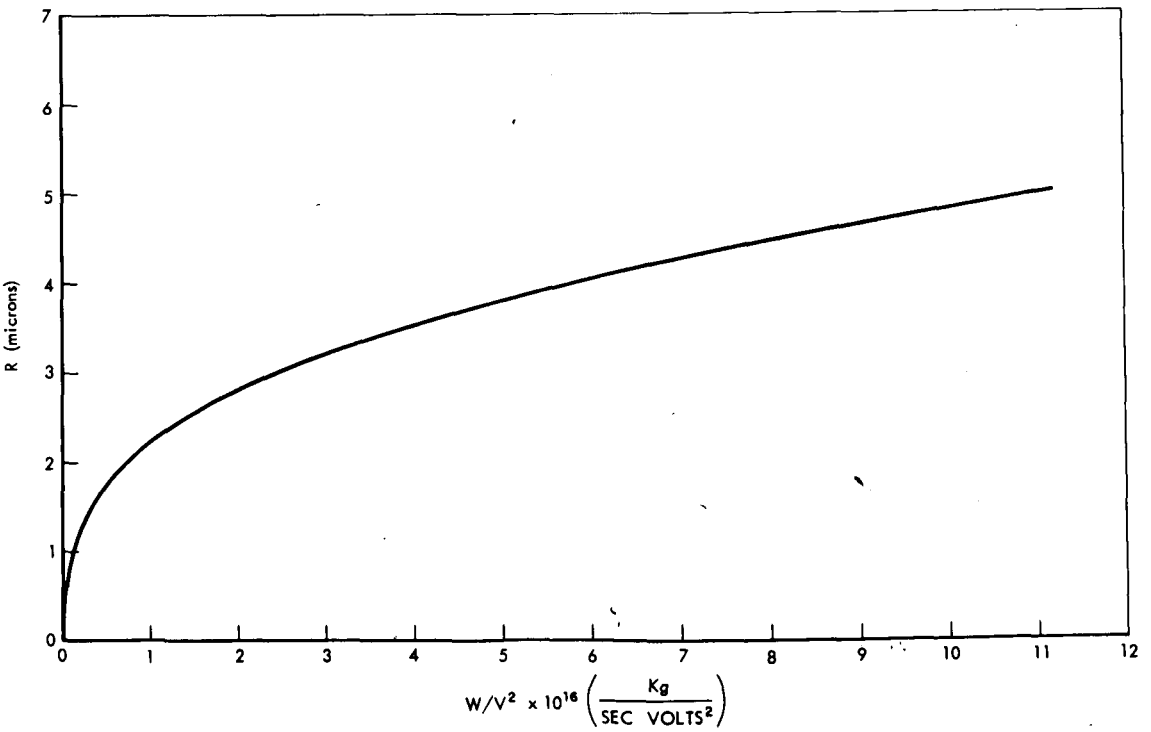

Figure 10. Droplet Radius vs Flow-Voltage Parameter

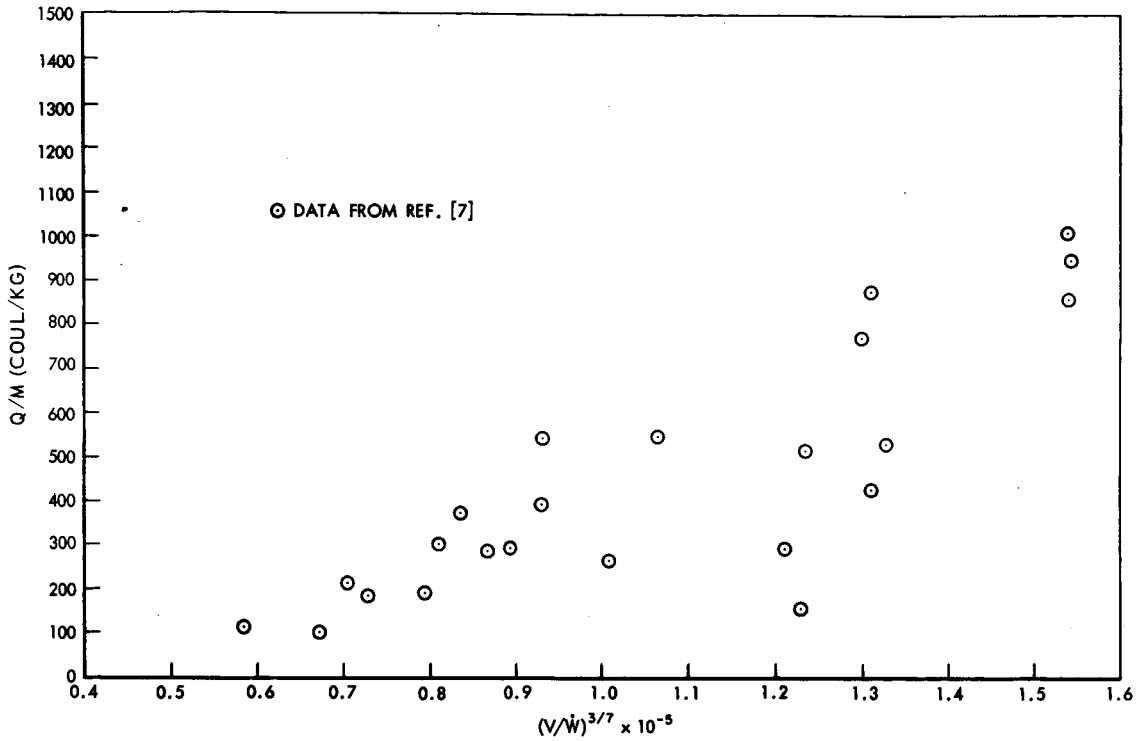

Figure 11. Charge-to-Mass Ratio vs Flow-Voltage Parameter, Computed According to Pfeifer

Effect of Surface Tension

The parametric grouping of flow and voltage result from the assumed model for droplet formation and the constancy of G in equation (9). Identification of these parameters provides a realistic basis for comparing test data, as well as for reducing the number of required data points.

The factor G, as stated, is a function of the particular perturbation distribution across the surface of the fluid. Thus, G should be dependent upon fluid-surface tension.

The dependence of G on surface tension can be estimated by assuming that the perturbation mechanism is approximated by a small wave across the meniscus. The velocity c of the wave is related by

$$C = \sqrt{\frac{\sigma}{R_i \rho}} \quad [11] \tag{18}$$

where R_i is the radius of the wave crest, or perturbation.

The energy of the moving crest is

$$E = \frac{1}{2} mv^2 + 3V_0 \sigma/R_i \tag{19}$$

where m is the mass of the crest and V_0 is its volume.

Substituting expressions for the crest mass and volume in terms of fluid density and crest width, w, the energy is expressed by

$$E = \frac{7}{2} \pi R_i w\sigma \ . \tag{20}$$

Hence, for a given energy input, the crest radius is related to surface tension by

$$R_i \sim 1/\sigma \ . \tag{21}$$

Combining equations (21) and (18) yields

$$C \sim \sigma/\sqrt{\rho} \ . \tag{22}$$

The effect of a change in surface tension on N, the number of droplet growth sites per second, is: For wave radii meeting the requirement for perturbation growth set by equation (6), N should vary directly and in proportion to the wave frequency. Hence,

$$f = C/\lambda \sim \frac{\sigma/\sqrt{\rho}}{\lambda} \ . \tag{23}$$

The wavelength, λ, is directly proportional to R; thus, combining (21) with (23):

$$f \sim \sigma^2 \ . \tag{24}$$

The factor K is proportional to σ^2 (with G proportional to σ^3) and, by the definition of K_1 in equation (14),

$$Q/M \sim \sigma^{4/3} \quad . \tag{25}$$

From equation (21) an increase of surface tension reduces the wave radii. Hence, some radii above the critical value (equation (6)) will be reduced enough so the perturbations will meet the growth requirements. Hence, Q/M will increase by a greater amount than indicated by equation (25).

In summary, the effect of surface tension on Q/M for a given voltage-flow parameter can be approximated by equation (25). Again, little data are available for correlation. However, the data in Figure 8 show an exponential dependence on Q/M on σ of about 1.1. Thus, the analytical estimation of the exponential dependence is high when compared with these data.

Variations in Electric Field and Q/M

In this analysis, variations in electric-field intensity or droplet charge-to-mass ratio across the liquid surface are not considered; average values are always considered.

For the data correlated in Figure 6, the beam efficiency varied from 69.9 to 95 percent; for the data in Figure 8, the beam-efficiency range was from 70.3 to 80.2 percent. Within these ranges, the assumption of an average charge-to-mass ratio appears to be good.

Fluid Electrical Conductivity

An initial assumption in the analysis was that the fluid conductivity is less than 10^{-5} mho/cm. Nevertheless, the derived flow-voltage parameter was shown to be valid in the 10^{-4} mho/cm range.

Changing the fluid electrical conductivity does not appear to change the flow-voltage parameter, but raises or lowers the floating constant K_1.

K_1 also probably depends on the shape of the capillary lip and the fluid-metal contact angle. Thus, the difficulty in obtaining a general solution for Q/M is apparent.

CONCLUSIONS

The analysis described here has validated the theoretical model, at least within the ranges of the data presented. The model serves to identify parametric groupings of voltage and flow to determine Q/M, v, and R. These parameters, as well as the factor G, provide a basis for comparing colloid dispersion data, for reducing number of data points, and for predicting performance within groups of tests.

REFERENCES

1. Drozin, V.: J. Colloid Science 10, 158-164 (1955)

2. Henriquez, P. C.: Rec. Trav. Chim 54, 574 (1935)

3. Onsager, L.: Am. Chem. Soc., 58, 1486 (1936)

4. Abraham, A., and Becker, R.: "The Classical Theory of Electricity and Magnetism," P. 101, Blackie and Son, Ltd., London, 1946

5. Neubaner, R., and Vonneyut, R.: J. Colloid Science 8, 851 (1953)

6. Cohen, E., and Huberman, M.: "Research on Charged Particle Electrostatic Thrusters," AFAPL-TR-66-94 (1966)

7. Cohen, E.: "Experimental Research to Determine the Feasibility of a Colloid Thruster," AFAPL-TR-65-72 (1965)

8. Pfeifer, R.: "Parametric Studies of Electrohydrodynamic Spraying," Report No. CPRL-4-65, Charged Particle Research Laboratory, University of Illinois

9. Hendricks, C., and Pfeifer, R.: "Parametric Studies of Electrohydrodynamic Spraying," AIAA Paper No. 66-252 (1966)

10. Wineland, S., Burson, W., and Hunter, R.: "The Electrodynamic Generation of Charged Droplet Beams," AFAPL-TR-66-72

11. Prandtl, L.: "Essentials of Fluid Dynamics," Hafner Publishing Co., 1952